NAVAL POSTGRADUATE SCHOOL

MONTEREY, CALIFORNIA

THESIS

HORIZONTAL ANISOTROPY AND SEASONAL VARIATION OF ACOUSTIC FLUCTUATIONS OBSERVED DURING THE 2010–2011 PHILIPPINE SEA EXPERIMENT

by

Bambang Marwoto
December 2015

Thesis Advisor: John A. Colosi
Second Reader: John Joseph

THIS PAGE INTENTIONALLY LEFT BLANK

REPORT DOCUMENTATION PAGE			Form Approved OMB No. 0704–0188
Public reporting burden for this collection of information is estimated to average 1 hour per response, including the time for reviewing instruction, searching existing data sources, gathering and maintaining the data needed, and completing and reviewing the collection of information. Send comments regarding this burden estimate or any other aspect of this collection of information, including suggestions for reducing this burden, to Washington headquarters Services, Directorate for Information Operations and Reports, 1215 Jefferson Davis Highway, Suite 1204, Arlington, VA 22202-4302, and to the Office of Management and Budget, Paperwork Reduction Project (0704-0188) Washington, DC 20503.			
1. AGENCY USE ONLY ***(Leave blank)***	**2. REPORT DATE** December 2015	**3. REPORT TYPE AND DATES COVERED** Master's thesis	
4. TITLE AND SUBTITLE HORIZONTAL ANISOTROPY AND SEASONAL VARIATION OF ACOUSTIC FLUCTUATIONS OBSERVED DURING THE 2010–2011 PHILIPPINE SEA EXPERIMENT			**5. FUNDING NUMBERS**
6. AUTHOR(S) Bambang Marwoto			
7. PERFORMING ORGANIZATION NAME(S) AND ADDRESS(ES) Naval Postgraduate School Monterey, CA 93943-5000			**8. PERFORMING ORGANIZATION REPORT NUMBER**
9. SPONSORING /MONITORING AGENCY NAME(S) AND ADDRESS(ES) N/A			**10. SPONSORING / MONITORING AGENCY REPORT NUMBER**
11. SUPPLEMENTARY NOTES The views expressed in this thesis are those of the author and do not reflect the official policy or position of the Department of Defense or the U.S. government. IRB Protocol number ____N/A____.			
12a. DISTRIBUTION / AVAILABILITY STATEMENT Approved for public release; distribution is unlimited			**12b. DISTRIBUTION CODE**

13. ABSTRACT (maximum 200 words)

The anisotropic ocean environment will lead to variability of ocean acoustic travel time. The variability of travel times comes from several ocean dynamical processes, including eddies, internal tides, and stochastic internal waves. This study analyzes time series of travel time from the Philippine Sea 2010–2011 experiment conducted by the Scripps Institution of Oceanography. In this experiment, a pentagonal array of acoustic transceivers of radius 600-km transmitted 250 Hz pulses for the purpose of observing acoustic variability at multiple time and space scales. Using filtering methods, this study separates variability in travel time in bands associated with eddies, internal tides, and stochastic internal waves. The observed fluctuations in the internal wave band are compared to a simple theoretical model.

The result of the research shows that over the year, eddies induce the largest amount of variability. Internal tides and internal waves show comparable fluctuations. There is some seasonal variability. Eddies and internal waves show fluctuations that are fairly isotropic across the array, while internal tides give highly anisotropic fluctuations. This anisotropy is related to the strong directionality of the internal tides that emanate from the Luzon Strait.

14. SUBJECT TERMS internal waves, ocean acoustic propagation, travel time variance, Philippine Sea			**15. NUMBER OF PAGES** 63
			16. PRICE CODE
17. SECURITY CLASSIFICATION OF REPORT Unclassified	**18. SECURITY CLASSIFICATION OF THIS PAGE** Unclassified	**19. SECURITY CLASSIFICATION OF ABSTRACT** Unclassified	**20. LIMITATION OF ABSTRACT** UU

NSN 7540–01-280-5500 Standard Form 298 (Rev. 2–89)
Prescribed by ANSI Std. 239–18

THIS PAGE INTENTIONALLY LEFT BLANK

Approved for public release; distribution is unlimited

HORIZONTAL ANISOTROPY AND SEASONAL VARIATION OF ACOUSTIC FLUCTUATIONS OBSERVED DURING THE 2010–2011 PHILIPPINE SEA EXPERIMENT

Bambang Marwoto
Lieutenant Commander, Indonesian Navy
S.T. in Hydrography, Indonesian Naval College of Science and Technology, 2007

Submitted in partial fulfillment of the
requirements for the degree of

MASTER OF SCIENCE IN PHYSICAL OCEANOGRAPHY

from the

NAVAL POSTGRADUATE SCHOOL
December 2015

Approved by: John A. Colosi
Thesis Advisor

John Joseph
Second Reader

Peter Chu
Chair, Department of Oceanography

THIS PAGE INTENTIONALLY LEFT BLANK

ABSTRACT

The anisotropic ocean environment will lead to variability of ocean acoustic travel time. The variability of travel times comes from several ocean dynamical processes, including eddies, internal tides, and stochastic internal waves. This study analyzes time series of travel time from the Philippine Sea 2010–2011 experiment conducted by the Scripps Institution of Oceanography. In this experiment, a pentagonal array of acoustic transceivers of radius 600-km transmitted 250 Hz pulses for the purpose of observing acoustic variability at multiple time and space scales. Using filtering methods, this study separates variability in travel time in bands associated with eddies, internal tides, and stochastic internal waves. The observed fluctuations in the internal wave band are compared to a simple theoretical model.

The result of the research shows that over the year, eddies induce the largest amount of variability. Internal tides and internal waves show comparable fluctuations. There is some seasonal variability. Eddies and internal waves show fluctuations that are fairly isotropic across the array, while internal tides give highly anisotropic fluctuations. This anisotropy is related to the strong directionality of the internal tides that emanate from the Luzon Strait.

THIS PAGE INTENTIONALLY LEFT BLANK

TABLE OF CONTENTS

THIS PAGE INTENTIONALLY LEFT BLANK

LIST OF FIGURES

THIS PAGE INTENTIONALLY LEFT BLANK

LIST OF TABLES

THIS PAGE INTENTIONALLY LEFT BLANK

ACKNOWLEDGMENTS

I wish to express my highest gratitude to God Almighty, because without God on my side, none of this would have been possible.

To my family, whose continuous support made me believe in myself,

To my friends,

To my Thesis Advisor John A. Colosi and Second Reader John Joseph,

To the chair of the Oceanography Department, Peter C. Chu,

To my academic associates, the late Mary Batteen and Ching-Sang Chiu,

To my program officers, Commander William Sommer and Commander Paula Travis,

To all the professors and staff of the Oceanography Department and Meteorology Department,

To my writing coach, Chloe Woida,

Thank you.

THIS PAGE INTENTIONALLY LEFT BLANK

I. INTRODUCTION

Acoustic propagation in the ocean is strongly influenced by the characteristics of the sea water and ocean dynamics. The circulation pattern of eddies, internal tides and internal waves are a few processes that determine the distribution of ocean sound speed and have a substantial impact on acoustic propagation.

Important among these processes are internal waves, which exist due to density stratification of the ocean. These waves randomly fill the oceans everywhere: there is never an internal calm. Internal waves alter the ocean sound speed field by vertically advecting water parcels. The resulting random internal-wave sound-speed structure then gives rise to acoustic scattering, thereby distorting and randomizing the acoustic field. This issue is common to many areas of wave propagation: Seismic propagation through the heterogeneous Earth, and optical propagation through the atmosphere (twinkling of stars) are two examples. Randomization of ocean acoustic signals can impose limitations on systems used for remote sensing, navigation, and communication and thus the study of this problem has many useful applications.

This thesis is concerned with a particular aspect of acoustic propagation through internal waves, namely their effects on signal travel time or acoustic phase. In this work, observations from the Philippine Sea will be examined, and theoretical modeling will be carried out to see if the observed statistics of travel time can be accurately predicted. The observed travel time statistics due to internal waves will be contrasted with travel time effects caused by internal tides and eddy.

A. NORTH PACIFIC ACOUSTIC LABORATORY (NPAL) IN PHILIPPINE SEA

This experiment is part of a series designed to capture any acoustic propagation variability related to oceanic and geographic conditions in the

Philippine Sea. The series began with the 2009 NPAL Pilot Study/Engineering Test (PhilSea09), and continued with the 2010–2011 NPAL Philippine Sea Experiment (PhilSea10) and the Ocean Bottom Seismometer Augmentation of 2010–2011 NPAL Philippine Sea Experiment (OBSAPS) (Worcester et al. 2013). This study concentrated on data from PhilSea10.

1. Objective of NPAL in Philippine Sea

The research was designed with several goals:

1. To learn the impact of eddies, internal tides, and random internal waves on acoustic propagation.
2. To develop better acoustic prediction methods, together with other measurements in the area.
3. To gain better understanding about how internal wave and spice affect acoustic propagation.
4. To characterize the depth and time dependence of ambient noise.
5. To understand the relationship between acoustics in the water column and seismic features of the ocean bottom

The study will further contribute to understanding of the impact of eddies, internal tides and internal waves on acoustic propagation areas. It will describe the variability of acoustic propagation travel time as a result of the influence of each of these ocean parameters. It will attempt to determine how variability changes with respect to seasonal changes and how it differs when the cyclone comes.

2. Research Location

The research placed a distributed vertical line array (DVLA) receiver surrounded by six transceiver stations (T1–T6) at various distances and relative directions from the DVLA. Geographical location of each station and the DVLA are shown in Figure 1, the coordinates are given by Table 1, and the distances between mooring stations are given by Table 2.

Figure 1. Location of Each Mooring during PhilSea10

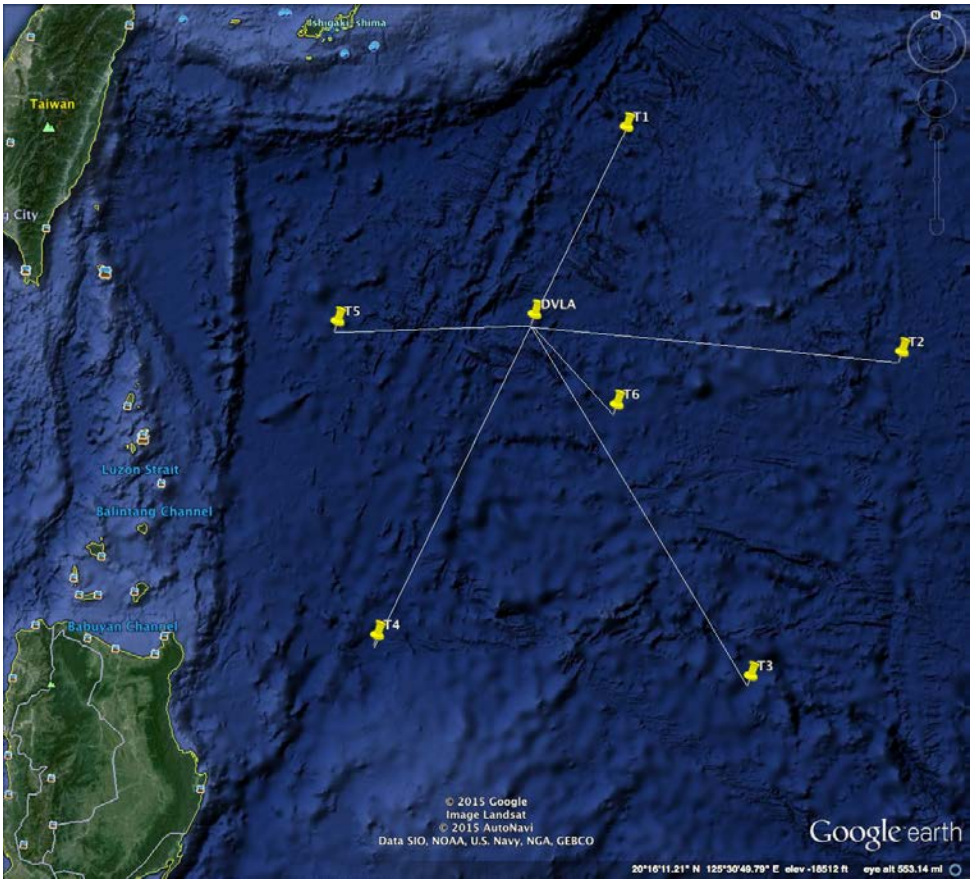

Transceiver station position calculated using reference WGS84. Adapted from: Google, 2015: *Philippine Sea*, 20°16'11.21" N and 125°30'49.79" E, Google Earth, accessed 21 June 2015.

Table 1. Location of Each Mooring during PhilSea10

	Location	
DVLA	21° 21.7418' N	126° 00.7867' E
T1	23° 08.3817' N	127° 04.0753' E
T2	20° 49.5130' N	129° 46.8332' E
T3	17° 47.2565' N	128° 03.4890' E
T4	18° 21.0740' N	124° 17.3629' E
T5	21° 21.9914' N	123° 59.2687' E
T6	20° 28.0546' N	126° 48.7610' E

Transceiver station position calculated using reference WGS84. Source: Worcester, P. F., Coauthors, 2013: The North Pacific Acoustic Laboratory deep-water acoustic propagation experiments in the Philippine Sea. *J.Acoust.Soc.Am.,* **134**, 3359–3375, doi:http://dx.doi.org/10.1121/1.4818887.

Table 2. Distance (km) between Stations with Reference WGS84 during PhilSea10

	T1	T2	T3	T4	T5	T6	DVLA
T1	0	379.66	601.46	603.93	373.28	297.05	224.84
T2		0	381.87	637.82	604.83	311.81	395.94
T3			0	403.81	582.46	324.3	450.13
T4				0	335.29	353.71	379.08
T5					0	310.25	210.06
T6						0	129.36
DVLA							0

Rhumb line distance between transceiver stations calculated with reference WGS84. Source: Worcester, P. F., Coauthors, 2013: The North Pacific Acoustic Laboratory deep-water acoustic propagation experiments in the Philippine Sea. *J.Acoust.Soc.Am.,* **134**, 3359–3375, doi:http://dx.doi.org/10.1121/1.4818887.

Figure 2. Acoustic Propagation Paths that Used in the Study

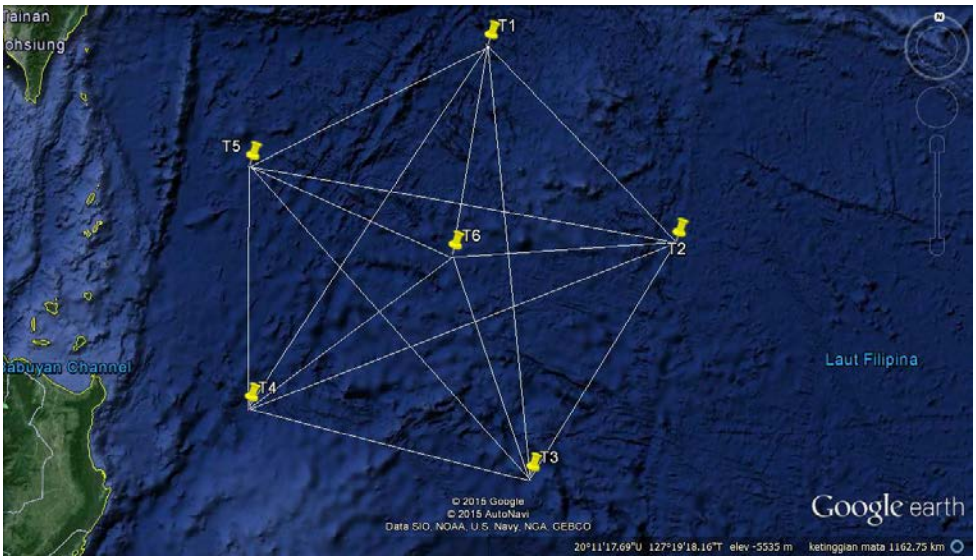

Ideal acoustic path used in the study. Signals were transmitted from T1, received by T2 – T6, transmitted from T2, received by others and continued until T5 transmission. The study could not use T6 transmission data due to the clock failure at T6 (Worcester et al., 2013). Adapted from: Google, 2015: Philippine Sea, 20°11'17.69" N and 127°19'18.16" E, Google Earth, accessed 21 June 2015.

The study will concentrate on the information related to propagation between each transceiver. DVLA information is not necessary to this study. Only

the information that transmits from one transceiver station and that is received by the other stations is calculated. There should be 30 path combinations (Figure 2), but because there was a clock problem at T6, the signal that originated from that station could not be processed. As a result, the study only used 25 path combinations, which originated from T1–T5.

3. Equipment Configuration

The DVLA recorded transmitted signals from all transceivers. It consisted of five subarrays. This array functioned to resolve low-order modes and characterized acoustic time front and ambient noise (Worcester et al. 2013).

The transmissions started from a near north position and moved in a clockwise direction. Transmission started from T1, followed by T2, through T6. The transceivers transmitted a 135-s linear frequency modulated (LFM) with bandwidth 100 Hz. Central frequencies that transmitted at every station were 250 Hz but for T2 the central frequency was 104–205 Hz. To avoid interference the transmission from each station was separated by nine minutes every hour (see Table 3) (Worcester et al. 2013). This nine-minute separation was chosen to give buffer time for the longest travel time calculated to be required for the longest distance. The longest distance between stations was 637.818 km, and the assumed sound speed in the ocean is 1,500 ms^{-1} (Pierce 1989); it takes seven minutes and five seconds for acoustic signal to travel from T2 to T4, and vice versa.

Table 3. Transceiver Bandwidth, Average Power Level and Transmission Time of Each Station during PhilSea10

Source	LFM Bandwidth (Hz)	Average Power Level (dB re 1μPa at 1m)	Transmission Time (min of the hour)	Source Depth (m)
T1	200 - 300	184.4	00	1068.7
T2	140 - 205	183.8	09	1070.1
T3	225 - 325	181.9	18	1062.4
T4	225 - 325	182.7	27	1064.6
T5	205 - 305	184.0	36	1061.7
T6	200 - 300	185.8	45	1066.0

There were four hydrophones installed above each transceiver. These hydrophones were installed at interval of nine meters. The hydrophones recorded the incoming signal from every transceiver. Even though T6 failed to transmit the signal, which affected to data supply for this study, it still recorded an incoming signal during the research. Adapted from: Worcester, P. F., Coauthors, 2013: The North Pacific Acoustic Laboratory deep-water acoustic propagation experiments in the Philippine Sea. *J.Acoust.Soc.Am.,* **134**, 3359–3375, doi:http://dx.doi.org/10.1121/1.4818887.

4. Environmental Information

The important environmental information for acoustic propagation is salinity, temperature and sound speed as a result. This section will give general information about environmental parameters during the research.

a. Salinity

The North Equatorial Current has contributed to establishing the lowest salinity near the surface; during summer, it is 34psu at 50m depth, and during other seasons, it is 34.2psu. North Pacific Tropical Water contributes to the highest salinity, 34.8psu at 150 to 250m depth. North Pacific Intermediate Water gives minimum salinity of 24.2psu at the depth of 500 to 650m (Rudnick et al.

2011). Weak spice at the depth of 800 to 1600m suggests there is an isopycnals layer (Colosi et al. 2013). After that depth, the salinity tends to remain constant (Figure 3, middle panel).

b. Temperature

Within the first hundred meters of depth, the average temperature in the summer in this area is about 30ºC, and during winter, is about 26ºC. The isothermal layer starts below 700m with 5ºC (Rudnick et al. 2011). See Figure 3, left panel.

Figure 3. Annual Average Temperature, Salinity and Sound-Speed Profiles at 21.36 N, 126.02 E

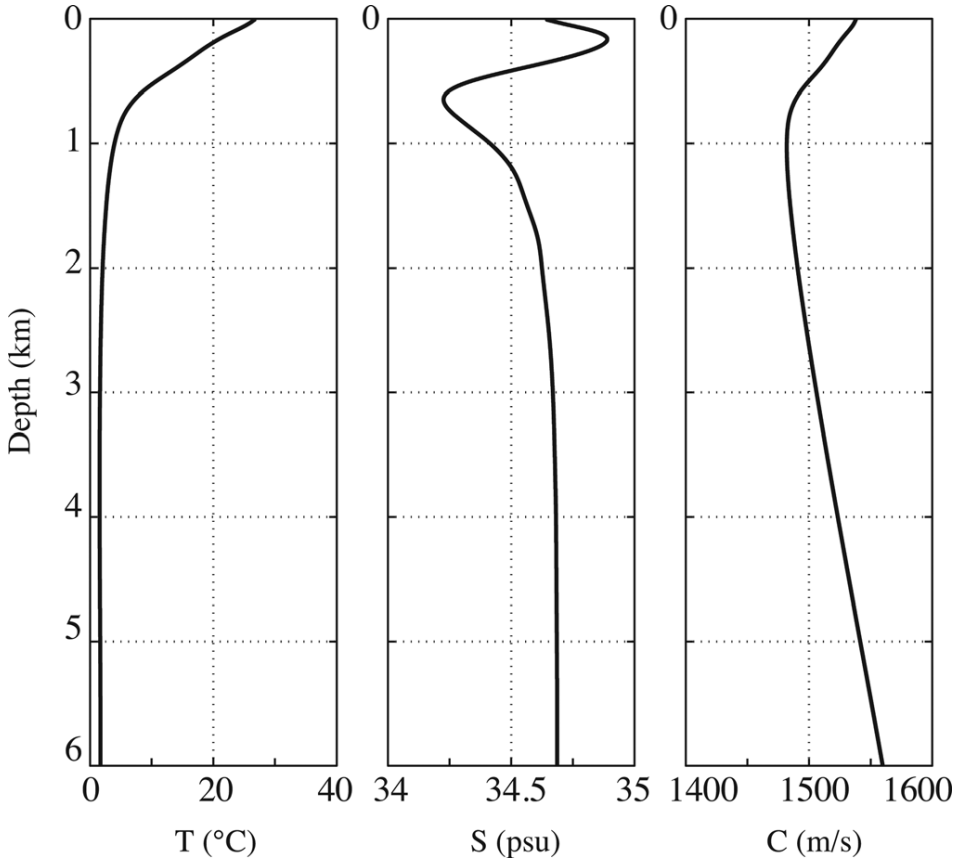

Average temperature, salinity and sound speed approximation at the locations of the PhilSea10 DVLAs, as derived from the World Ocean Atlas 2005. Source: Worcester, P. F., Coauthors, 2013: The North Pacific Acoustic Laboratory deep-water acoustic propagation experiments in the Philippine Sea. *J.Acoust.Soc.Am.,* **134**, 3359–3375, doi:http://dx.doi.org/10.1121/1.4818887.

c. Sounds-Speed Profile

Sound-speed profiles tend to create a sound channel at an axis depth around 1000m (Figure 3, right panel). The depth of the ocean sufficient to locate the critical depth above the ocean bottom (Worcester et al. 2013). This makes observation easier because boundaries of the ocean do not interfere with the propagation of the sound wave.

B. OBJECTIVE OF STUDY

This study used data that had been processed by Scripps Institute of Oceanography, University of California San Diego. The study concentrated on the statistics of acoustic travel time during research periods, and tried to extract information about

- overall travel time variance caused by internal waves, internal tides and eddies;
- scaling of travel time variance with range;
- changes in travel time variance with season;
- comparison with acoustic models for travel time variance using the Garrett-Munk internal wave spectrum;
- horizontal anisotropy of travel time variance (e.g., is the variance larger in a particular direction?); and
- effects of Typhoons on travel time variance.

C. NAVY RELEVANCE

Knowing acoustic propagation variability can help sonar operators to determine sonar detection accuracy. The variability of acoustic propagation can describe means and error bars for terms in the sonar equation. Predicting acoustic variability required a detailed knowledge of the ocean environment.

II. OCEAN ACOUSTIC PROPAGATION

This chapter will discuss acoustic wave propagation through the ocean using ray theory. The focus is to describe wavefront propagation in the ocean sound channel and to discuss the variability of ray travel times along different sections of the wavefront.

Because attenuation is weak, low frequency acoustic waves can be detected and utilized at very long distances in the ocean. This study will use ray theory to describe how acoustic waves behave during their propagation. Ray theory is used because of its simple geometric interpretation and because we are concerned with the acoustic variable of travel time, which is well described by ray theory even in a stochastic environment (Colosi 2015, manuscript submitted for publication to Cambridge University Press).

There are several ways to interpret ray theory both mathematically and conceptually. One useful approach is to assume that locally an acoustic wave looks like a plane wave. In this approach, the rays are understood as lines that run perpendicular to the wave front. These rays will describe the path of the acoustic wave during its propagation. The paths are dictated by refraction and reflection. There is no diffraction in ray theory. Since reflection only occurs at the boundaries, refraction is the key physical process for deep water long range propagation through the ocean at low and middle latitudes. Variations in sound speed give variation to ray refraction.

For a plane wave, the wavenumber and frequency are related to the wave phase by $\vec{k} = \nabla\theta$ and $\omega = -\frac{\partial\theta}{\partial t}$. Taking the divergence of the frequency we obtain

$$\frac{\partial\vec{k}}{\partial t} = -\left(\frac{\partial\omega}{\partial\vec{k}} \bullet \nabla\right)\vec{k} - \frac{\partial\omega}{\partial\vec{r}} \tag{2.1}$$

Here $\frac{\partial \omega}{\partial \vec{k}}$ is seen to be the group speed, and the total derivative along the ray is $\frac{\partial}{\partial t} + c_g \bullet \nabla$. Rewriting this equation using the total derivative gives the refraction equation:

$$\frac{d\vec{k}}{dt} = -\frac{\partial \omega}{\partial \vec{r}} \tag{2.2}$$

This equation tells us how the wavenumber changes direction. Identifying the group speed as the rate of change of position of the ray, we then also have the equation:

$$\frac{d\vec{r}}{dt} = \frac{\partial \omega}{\partial \vec{k}} = \vec{c}_g \tag{2.3}$$

These two vector equations give us six coupled scalar equations for six unknowns, which are three components of the wavenumber and three components of the position all as a function of time.

Here we need the dispersion relation for acoustic waves, which is given:

$$\omega\left(\vec{r},\vec{k}\right) = \left(k_x^2 + k_y^2 + k_z^2\right)^{1/2} c\left(\vec{r}\right) \tag{2.4}$$

In these equations, k_x, k_y, k_z are the wave numbers along each axis and $c\left(\vec{r}\right)$ is the three dimensional sound speed. If c is a function of z, the dispersion relation becomes $\omega = \left(k_h^2 + k_z^2\right)^{1/2} c\left(z\right)$, where k_h is constant. In this case Snell's law gives $\frac{\cos\theta}{c} = cons$. Making x the independent variable and considering a 2-d problem in the x-z plane, the ray equations are:

$$\frac{dz}{dx} = \frac{\partial H}{\partial p_z} \tag{2.5}$$

$$\frac{dp_z}{dx} = -\frac{\partial H}{\partial z} \tag{2.6}$$

$$\frac{dT}{dx} = L = p_z \frac{dz}{dx} - H = \frac{1}{c^2\left(c^{-2} - p_z^2\right)^{1/2}} = \frac{\sec\theta}{c} \tag{2.7}$$

In these equations, the new quantity of $p_z = \frac{k_z}{\omega} = \frac{\sin\theta}{c}$ is the vertical wave slowness; $H = -\frac{k_x}{\omega} = -\left(c^{-2} - p_z^2\right)^{1/2} = -\cos\frac{\theta}{c}$ is the Hamiltonian function; and L is Lagrangian function. Equation (2.7) simply tells us that the acoustic waves move at the local sound speed.

In this study, we will consider source depths close to the sound channel axis, which for the Philippine Sea is about 1000 m depth. Consider first the case c=c(z). As rays leave the source, they arrive in an environment, which has higher sound speed propagation. As a consequence of Snell's Law, each ray will bend away from the normal line. At some point the ray begins to move in the opposite direction from its original direction at the source and the ray starts to bend back toward the normal line. This pattern is repeated all along the path of the ray. The upper limit at which the ray starts moving downward is known as the upper turning point (z^+); the other change at the lower limit is called the lower turning point (z^-). As a result of this process the ray will remain within the corridor between the upper limit and the lower limit. In this study, the ray will remain within a corridor with an axis at around 1,000 m depth.

There is a method to differentiate and to identify the ray paths, using the grazing angle (θ_g). θ_g is the angle that is measured from the axis of acoustic propagation to a particular path being identified. Mathematically θ_g can be determined by Snell's law:

$$\cos(\theta_g) = \frac{c_{axis}}{c_{turn}} \tag{2.8}$$

In this equation, c_{axis} is sound speed at the axis of propagation and c_{turn} is sound speed at the particular depth of the ray turning point in which we are interested (Figure 4).

Figure 4. Sketch Ray Propagation around the Axis

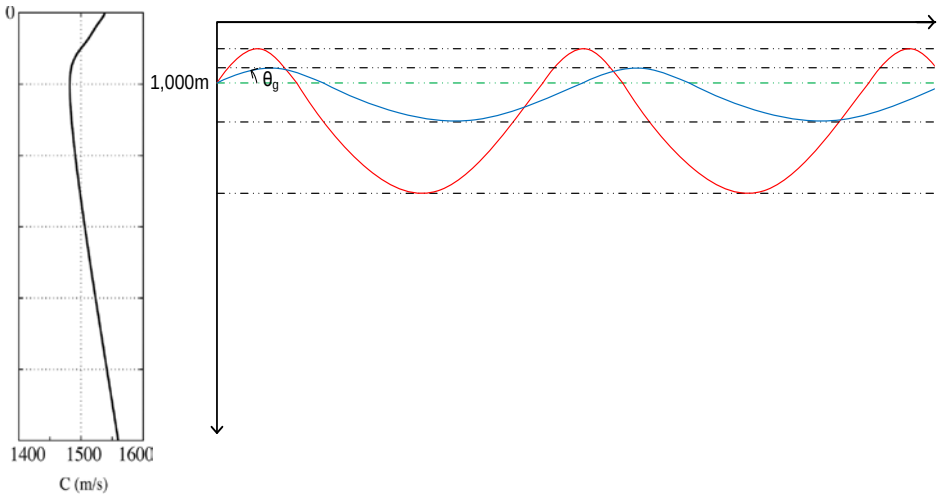

The left panel of the figure is the vertical sound speed profile from Chapter I, Figure 3. The right panel shows that the rays that have a higher grazing angle (red line) will reach a higher sound speed depth; the rays that have a lower grazing angle cannot reach the same depth.

Figure 5. Ray ID15 of T4-T5

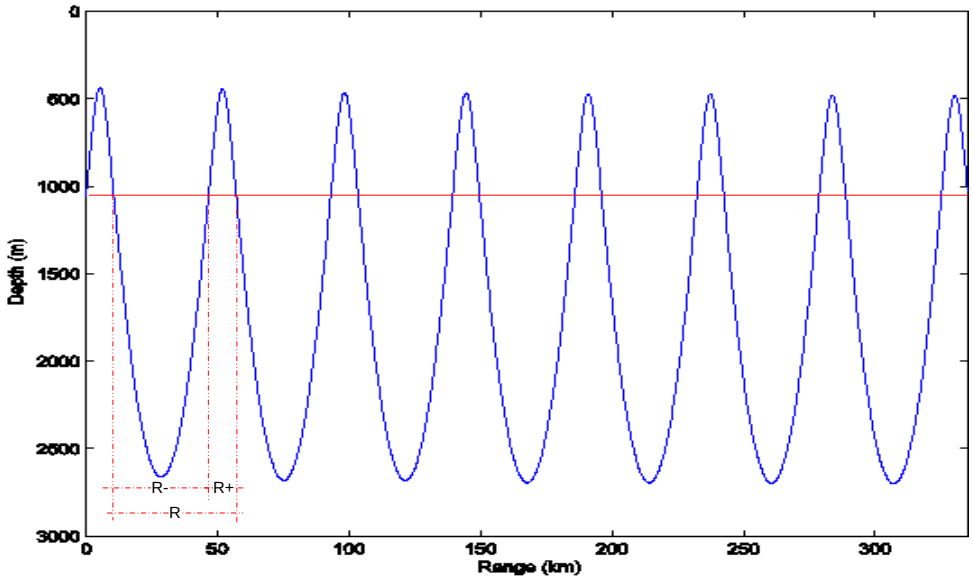

This ray originated from T4 and was received by T5. It was given the ID number ID+15 because it left the source (left border of figure) going upward, and it had 8 upper turning points and 7 lower turning points or a total of 15 turning points. The R is the horizontal ray cycle distance. R+ is the horizontal distance of the upper loop, and R- is the horizontal distance of the lower loop.

Another way to distinguish one ray from another for a given sound speed profile and a set receiver depth and range is the ray identification (ID) number. Each ray will be given a specific identification number. The number will represent how many turning points the ray has before it reaches the receiver. The sign (+ or -) of the ID indicates whether the ray went upward (+) or downward (-) from the source. For example ID +15 shows us that the ray left the transmitter upward and had 15 turning points before it reached the receiver. The ID-15 shows us that the ray left the transmitter downward and had 15 turning points (Figure 5).

Figure 6. Ray Plotting of Two Rays for the Study

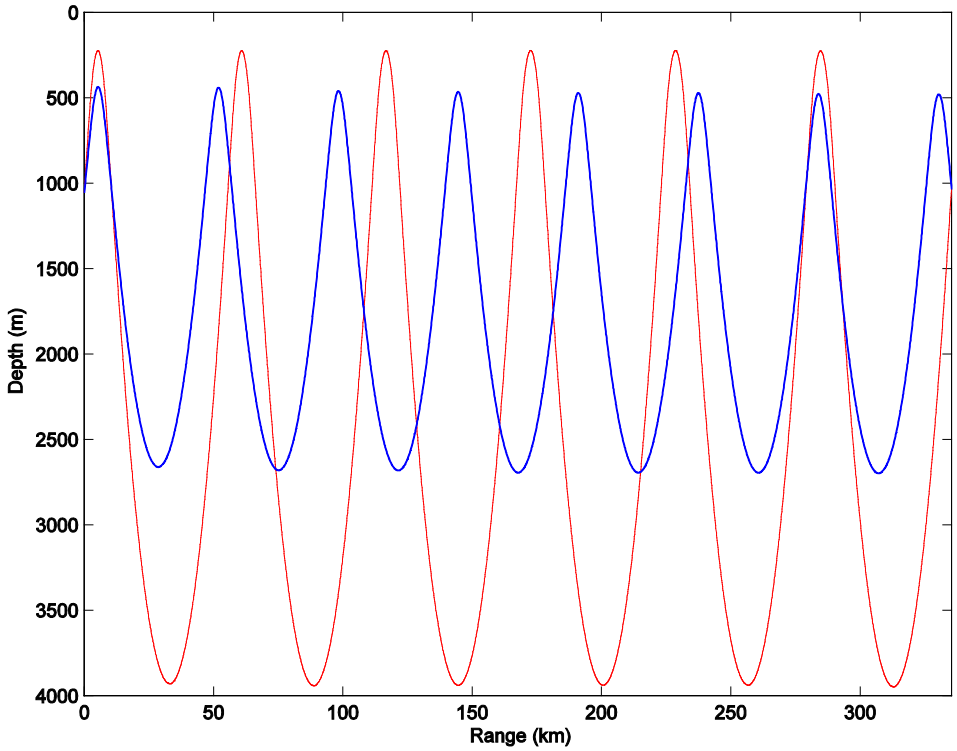

The plotting of the transmission of two rays transmitted from T4 to T5. Red represents a ray with ID+12, which has the largest grazing angle and 12 turning points. A ray with a smaller grazing angle, represented by blue, had 15 turning points, and an ID+15. The red ray traveled a longer distance than the blue ray. Any ray with an odd ID number will reach the receiver in the same direction as it left the transmitter, while a ray with an even ID number will reach the receiver from the opposite direction.

Ray loop distances, defined as the horizontal distance traveled by a ray over an up/down cycle of the ray, are a function of grazing angle, and for a mid-latitude profile like the Philippine Sea, ray loop distance increases with grazing angle. This means that higher grazing angle rays will be associated with smaller IDs.

The rays that departed from the source and arrive at a fixed receiver depth at fixed range are called eigenrays (Figure 6). During propagation, acoustic signals follow many different paths or eigenrays. This situation is known as multipath propagation.

Figure 7. Travel Time of Some Rays from T4-T5 Transmission

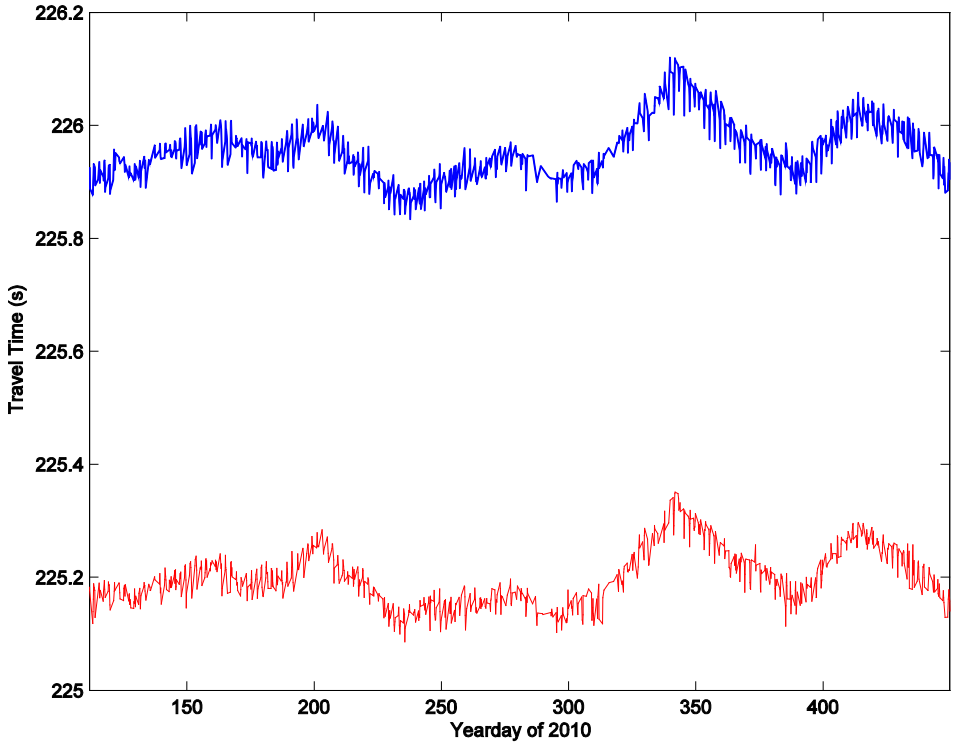

Blue represents ID15 and red represents ID12. The horizontal axis shows the year day of 2010 and the vertical axis shows the travel time in seconds. The research data show that, throughout the research period, rays with higher grazing angles (red) had faster travel time than rays with lower grazing angles (blue).

In mid-latitude sound speed profiles higher grazing angle rays (with smaller IDs) have a larger horizontal group speed than low angle rays. The research data give some proof of this (Figure 7). The eigenray with a higher grazing angle (red ray, ID12) has an earlier travel time than the lower grazing angle eigenray (blue ray, ID15).

A. TIME FRONT

Wave fronts are difficult to observe because instrumentation would be required in the (x,z) plane. An easier observational arrangement is to place a set of vertical receivers at a fixed range and record the wavefront sweeping by the receivers in time. This is called a time front, yielding data in the (z,t) plane. This is the arrangement for the Philippine Sea data.

Figure 8. Time Front Illustration

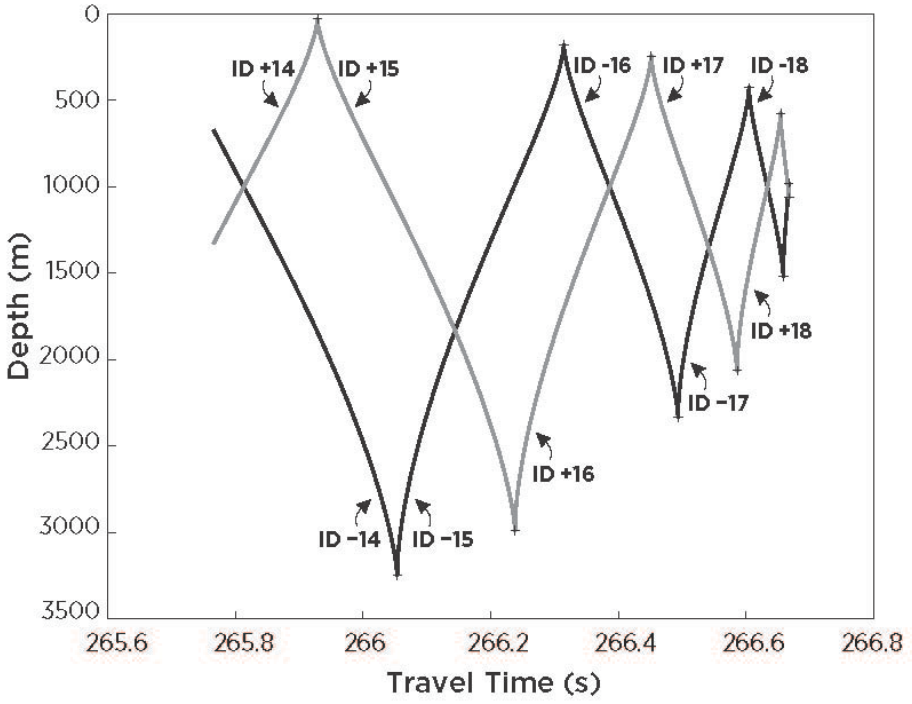

Time front for the Munk canonical profile for range 400km. The x-axis is travel time and the y-axis is depth. Source: Colosi, J. A., 2015: Sound propagation through the Stochastic Ocean [manuscript submitted for publication].

The previous section gave information about how a ray with a higher grazing angle will a have smaller ID number, a shallower upper turning point, and a deeper lower turning point. A ray with a lower grazing angle has the opposite. As a result, the rays with higher grazing angles will arrive at the receiver first and at a wide span of depth, while rays with lower grazing angles will arrive later with a narrower span of depth.

Figure 9. One of Time Front Plotting Data from the Research

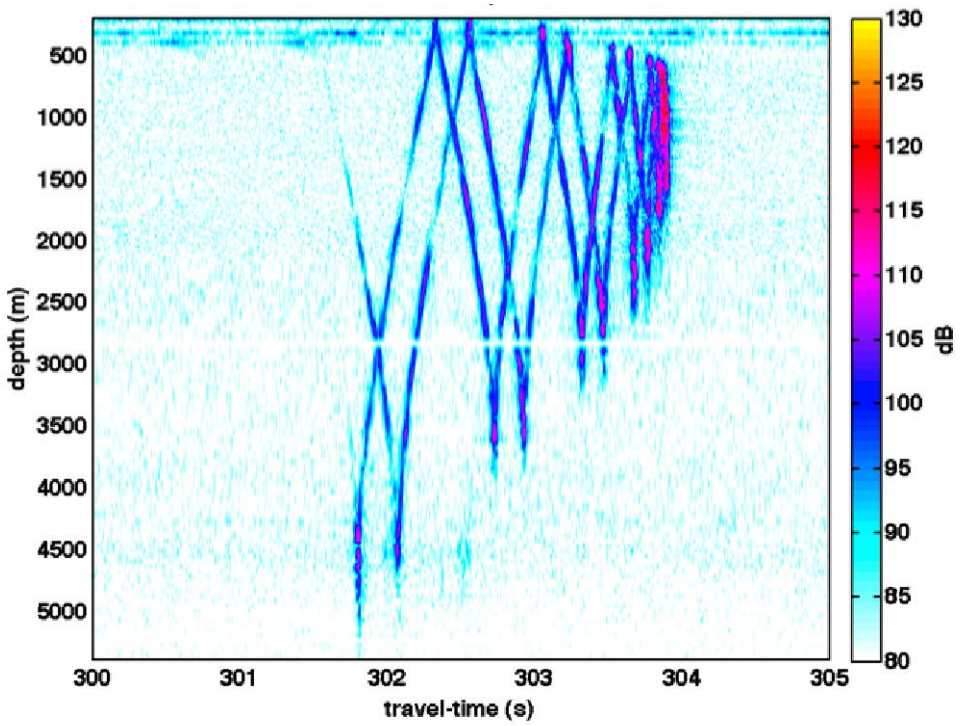

The x-axis shows the travel time from the transmitter to the receiver. The y-axis shows the depth where the ray arrived at the receiver. The color gives information about the strength of acoustic power in dB. Source: Colosi, J. A., 2015: Sound Propagation through the Stochastic Ocean [manuscript submitted for publication].

Plotting the travel time from research data, we have the same profile with Figure 8. The earlier arrivals are rays with higher grazing angle, and with weak acoustic intensity. The later arrivals are rays with smaller grazing angles with higher intensity. Figure 9 shows them.

B. TRAVEL TIME VARIANCE: RAY THEORY

This research considers the source and the receiver at a fixed range. The rays, therefore, will all travel the same horizontal distance. The eigenrays will have different grazing angles and different wavefront IDs. The eigenray paths differ and are therefore influenced by different sound speed structure. Ocean structure, due to internal waves, internal tides, and eddies, will cause the eigenrays to wander randomly in time. The variance of this wander is a statistic of great importance.

To predict the travel time variance we can use ray theory since diffraction has little influence on travel time.

For a straight line ray, the delay or advance of the travel time due to a sound-speed difference (δc) is written using ray theory as:

$$T = \left[\int_0^R \frac{1}{c_0 + \delta c} dx - \int_0^R \frac{1}{c_0} dx \right] \tag{2.9}$$

In Equation (2.9), the c_0 is the background sound speed. Carrying out a binomial expansion, the travel time deviation from Equation (2.9) will be:

$$dT = -\int_0^R \frac{\delta c}{c_0^2} dx \tag{2.10}$$

In Equation (2.10), $\frac{\delta c}{c_0}$ is known as fractional sound speed variance. It has symbols μ and a function of x. The travel time variance is given by:

$$\tau^2 = \left\langle dT^2 \right\rangle \tag{2.11}$$

The travel time variance also can be determined by calculating the ratio of log amplitude variance to the sound speed reference square, as shown:

$$\tau^2 = \frac{\left\langle \chi^2 \right\rangle}{c_0^2} \tag{2.12}$$

In Equation (2.12), the $\left\langle \chi^2 \right\rangle = \Phi^2 / k_0^2$ where Φ is the phase variance and k_0 is the wave number of acoustic signal. Furthermore, because the k_0 is equal to ω / c_0, the Equation (2.12) become:

$$\tau^2 = \frac{\Phi^2}{\omega^2} \tag{2.13}$$

From Munk and Zachariasen (1976) Theory, we have:

$$\Phi^2 = k_0^2 \int ds \left\langle \mu^2 \right\rangle L_p \tag{2.14}$$

In Equation (2.14), $\left\langle \mu^2 \right\rangle$ is fractional sound speed variance as a function of ray depths, which gives information how the sound speed change compare to sound speed reference given by $\left\langle \delta c^2 \right\rangle / c_0^{\,2}$; L_p is correlation length of internal wave in the direction of acoustic wave as a function of ray grazing angle and depth.

Sound speed distribution in the ocean space is important factor for acoustic wave propagation in the ocean. The distribution of the sound speed profile is controlled by the dynamic in the ocean. The next chapter will discuss some dynamics in the ocean that affect the acoustic propagation in the ocean.

III. OCEAN VARIABILITY

Some of the ocean dynamics that affect acoustic propagation in the ocean will be discussed in this chapter. We now take up the question of fluctuations in the ocean sound speed field and consider a model in which:

$$c(x,y,z) = \bar{c}(z) + \delta c(x,y,z) \tag{3.1}$$

This study concentrates on internal waves, the gravity waves that are supported by the continuous density stratification of the water column.

Internal waves can be generated at the surface, bottom, and interior of the ocean (Garrett and Munk 1975). The surface generation mechanism is associated with wind stress (Watson et al. 1976). These types of internal waves are categorized as inertial waves because of the strong response near the inertial period (Colosi 2015, manuscript submitted for publication to Cambridge University Press).

The bottom generation mechanism occurs when a strong current, like the barotropic tide, flows across different bottom topographic features, such as the continental shelf, sills, seamounts, and ridges (Bell 1975). Because of the common tidal generation force these waves are often called internal tides (Garrett and Kunze 2007). Associated with internal tides in shallow water are nonlinear internal waves called internal solitary waves (Colosi 2015, manuscript submitted for publication to Cambridge University Press). The interior generation mechanism is related to shear of currents in the ocean column (Muller 1976). In a poorly understood process, all these generation mechanisms in concert with nonlinear wave-wave interactions and Doppler smearing, give rise to a rich spectrum of random ocean internal waves that are observed virtually everywhere in the world oceans (Colosi 2015, manuscript submitted for publication to Cambridge University Press). These random waves are critical for acoustic propagation.

A. INTERNAL WAVE

Internal waves generate sound speed perturbations by vertical advection of the background sound speed structure:

$$dc(x,y,z,t) = \left(\frac{dc}{dz}\right)_p (z)\zeta(x,y,z,t) \tag{3.2}$$

In Equation (3.2), ζ is the vertical displacement and $\frac{dc}{dz}p$ is the potential gradient of sound speed which is needed due to the adiabaticity of the internal-wave motions.

The internal wave spectrum was described by Garrett and Munk (1972), and since then, many small improvements have been made. The model describes the ocean displacements as an integration of all possible internal waves (Colosi 2015, manuscript submitted for publication to Cambridge University Press).

$$\zeta(r,t) = \iiint \hat{\zeta}(\kappa)\, e^{i(\kappa \bullet r - \sigma(\kappa)t)} d\kappa \tag{3.3}$$

where $\hat{\zeta}$ are random internal wave amplitudes, and $\sigma(\kappa)$ is the dispersion relation, as described by Colosi (2015, manuscript submitted for publication to Cambridge University Press) the statistic of $\hat{\zeta}$ is as follows:

$$\left\langle \hat{\zeta}(\kappa) \right\rangle = 0 \tag{3.4}$$

$$\left\langle \hat{\zeta}(\kappa)\hat{\zeta}^*(\kappa') \right\rangle = F_\zeta(\kappa)\delta(\kappa - \kappa') \tag{3.5}$$

$$\left\langle \hat{\zeta}(\kappa)\hat{\zeta}(\kappa') \right\rangle = \left\langle \hat{\zeta}^*(\kappa)\hat{\zeta}^*(\kappa') \right\rangle = 0 \tag{3.6}$$

In Equation (3.5), the $F_\zeta(\kappa)$ is the displacement wave number spectrum with:

$$\left\langle \zeta^2 \right\rangle = \iiint F_\zeta(\kappa)\, d\kappa \tag{3.7}$$

The Garrett Munk spectrum can be written in terms of frequency and mode number (Colosi 2015, manuscript submitted for publication to Cambridge University Press):

$$F_{\zeta}(\sigma, j) = \zeta_0^2 \frac{N_0}{N(z)} B(\sigma) H(j) \tag{3.8}$$

In Equation 3.8, $B(\sigma)$ and $H(j)$ can described as follows:

$$B(\sigma) = \frac{4}{\pi} \frac{f\sqrt{\sigma^2 - f^2}}{\sigma^3} \tag{3.9}$$

$$H(j) = \frac{1}{N_j} \frac{1}{j^2 + j_*^2} \tag{3.10}$$

This model has slope as a power function of frequency and mode number with degree of -2.

B. INTERNAL TIDE

The internal tide is a tidally forced internal wave. These waves change the ocean sound speed field by vertical displacements, in the same way as random internal waves. Because there is no specific model to predict internal tides in the Philippine Sea, this thesis will not be able to make internal tide travel time estimates. In fact travel time fluctuations are often used to estimate the internal tide using the methods of ocean acoustic tomography (Dushaw 2008). Internal tides will be estimated from the data by applying least square tidal fits to the travel times collected in the time series data set.

The internal tides are important for the Philippine Sea because there are two submarine ridges along the Luzon Strait that generate internal tides. The ridges that comprise the Luzon Island Arc (Zhao 2014) have heights that vary, which critically affect both diurnal and semidiurnal internal tides (Farmer et al. 2009). Furthermore, the internal tide that is generated at the Luzon strait propagates over 2,500 km into the Philippine Sea (Zhao 2014).

The presence of internal tide impact has been observed during research. Colosi et al. (2013) using PhilSea09 data, found that strong fluctuations within diurnal periods arise in the data, as shown in Figure 10. Colosi's research used four tide harmonic constituents to observe the diurnal frequency, and four constituents for the semidiurnal frequency. The tide periodic constituent is the value that represents the effect on the tide period and amplitude due to periodic variation position of earth, sun and moon.

Figure 10. Observed Potential Density during PhilSea09

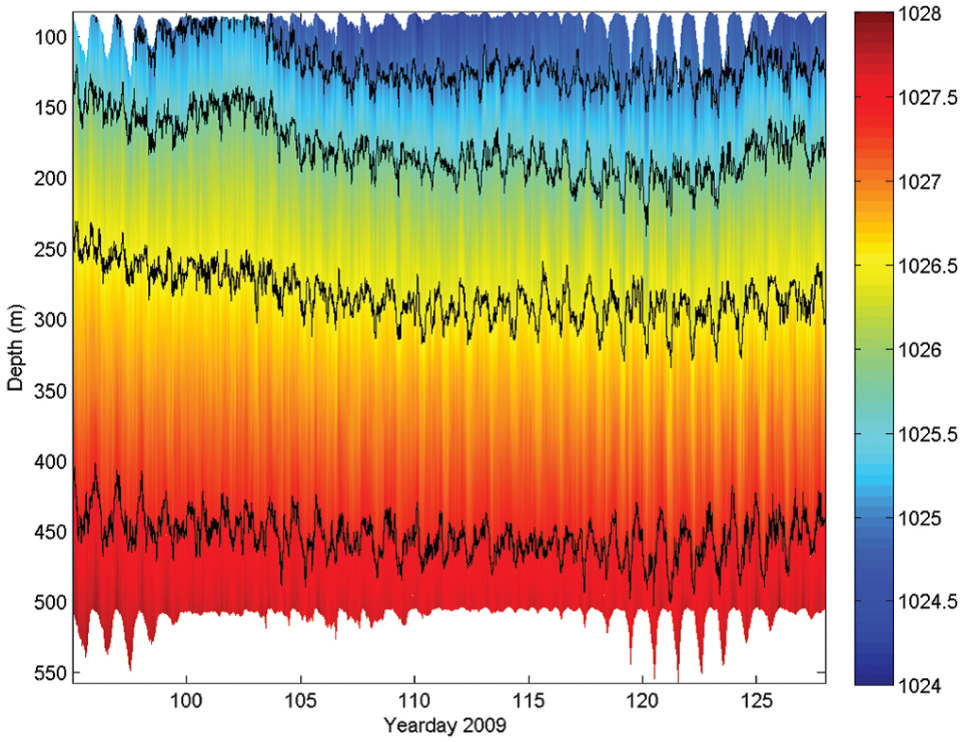

Observe potential density (σ_{300}) at DVLA. Source: Colosi et al., 2013: Observations of sound-speed fluctuations in the western Philippine Sea in the spring of 2009. *J.Acoust.Soc.Am.,* **134**, 3185–3200, doi:http://dx.doi.org/10.1121/1.4818784.

This study tries to estimate the effects of 13 tide harmonic constituents on travel time in order to eliminate the effect of these constituents on travel time variation. These harmonic constituents as presented by NOAA (2015) are M2

(principal lunar semidiurnal constituent), S2 (principal solar semidiurnal constituent), N2 (larger lunar elliptic semidiurnal constituent), K2 (lunisolar semidiurnal constituent), L2 (smaller lunar elliptical semidiurnal constituent), O1 (lunar diurnal constituent), K1 (lunar diurnal constituent), P1 (solar diurnal constituent), Q1 (larger lunar elliptic diurnal constituent), J1 (smaller lunar elliptic diurnal constituent), M3 (lunar terdiurnal constituent), M4 (shallow water over tides of principal lunar constituent) and M6 (shallow water over tides of principal lunar constituent). The period of each constituent is shown in Table 4.

Table 4. Periodic Constituents Eliminated from the Data

NOAA #	Constituent	Darwin Symbol	Period (hour)	Speed (°/hour)
1	principal lunar semidiurnal	M2	12.4206012	28.9841042
2	principal solar semidiurnal constituent	S2	12	30
3	larger lunar elliptic semidiurnal	N2	12.65834751	28.4397295
35	lunisolar semidiurnal	K2	11.96723606	30.0821373
33	smaller lunar elliptical semidiurnal	L2	12.19162085	29.5284789
6	lunar diurnal	O1	25.81933871	13.9430356
4	lunar diurnal	K1	23.93447213	15.0410686
30	solar diurnal	P1	24.06588766	14.9589314
26	larger lunar elliptic diurnal	Q1	26.868350	13.3986609
19	smaller lunar elliptic diurnal	J1	23.09848146	15.5854433
32	lunar terdiurnal	M3	8.280400802	43.4761563
5	shallow water over tides of principal lunar	M4	6.120300601	57.9682084
7	shallow water over tides of principal lunar	M6	4.140200401	86.9523127

Adapted from: NOAA, 2015: Harmonic Constituents for 9410170, San Diego CA. Available at http://tidesandcurrents.noaa.gov/harcon.html?id=9410170&type=.

C. EDDIES

Eddies become important for this study because typical currents for general ocean circulation are about 1 cm/s while for eddies the value is about 10 cm/s (Flatte 1979). This condition reveals that about 99% of the kinetic energy of the ocean is contained in eddies.

The eddies in the ocean are generally formed by one of two processes: 1) instability of a swiftly moving current such as a Western boundary current or, 2)

flow over and around topographic features such as points, continental shelf breaks, and slopes.

Eddies have a typical length scale of about 100 km, and a typical time scale of about 2 months. In the research area, the Philippine Sea, the eddies can extend as deep as 1,000 m and have a dominant time scale of 100 days (Qiu and Chen 2010). The strong eddies that move across the sea from east to west modulate the sound speed fields in the research area (Qui and Chen 2010).

Figure 11. The Presence of Eddies at Study Area

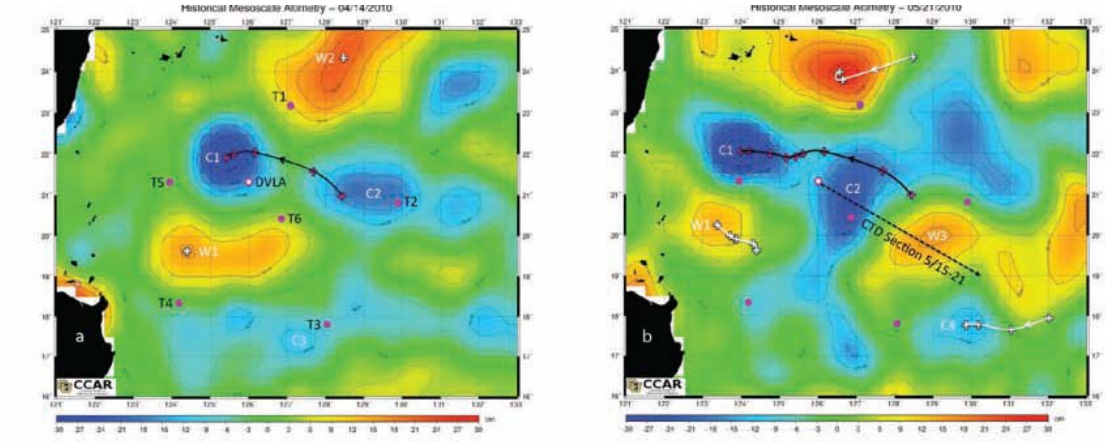

The left panel shows historical altimetry data taken at 14 Apr 2010 and the right panel shows historical altimetry data taken at 21 May 2010. The transducer station and DVLA station are marked as pink dots. The cold core eddies are labeled with c1 to c4, and the warm core eddies are labeled with w1 to w3. Source: Ramp, S. R., et al., 2014: Direct observations of the mesoscale variability in the western Philippine Sea [manuscript submitted for publication].

Warm core eddies (anticyclonic) and cold core eddies (cyclonic) both are present in the study area. On average the warm eddies are larger and more elliptical than the cold eddies. The warm eddies have an average major axis of 385 km and an average minor axis of 211 km, while the cold eddies have an average major axis of 301 km and an average minor axis of 227 km (Ramp et al. 2014, manuscript submitted for publication to *J.Phys.Oceanogr*). As shown in Figure 11 the presence of eddies during the research was not static; they were affected by the general circulation of the ocean. The cold core eddies are

supplied from the North Pacific Intermediate Water coming to the research area from the northeast as a part of North Pacific Gyre (Nakano et al. 2005); the warm core eddies are supplied by North Pacific Tropical Water (Rudnick et al. 2011).

Ocean dynamics control ocean acoustic travel time variabilities. The ocean acoustic travel time variabilities of the Philippine Sea during the research period will be explained in the next chapter.

THIS PAGE INTENTIONALLY LEFT BLANK

IV. OBSERVED TRAVEL TIME STATISTICS

This chapter describes how travel time variability in the Philippine Sea during the research period changed with respect to season, dominant direction of signal, and typhoon activity. Travel time data that the study received from the research reflected the influence of eddies and tide. Observed travel times of the signal transmitted from T4 and received by T5 throughout the research period clearly show that there is some tidal effect in the travel time data (Figure 12). The previous chapter discussed filtering methods for eliminating the effect of tides and eddies from the data.

Figure 12. Travel Time throughout the Research Period

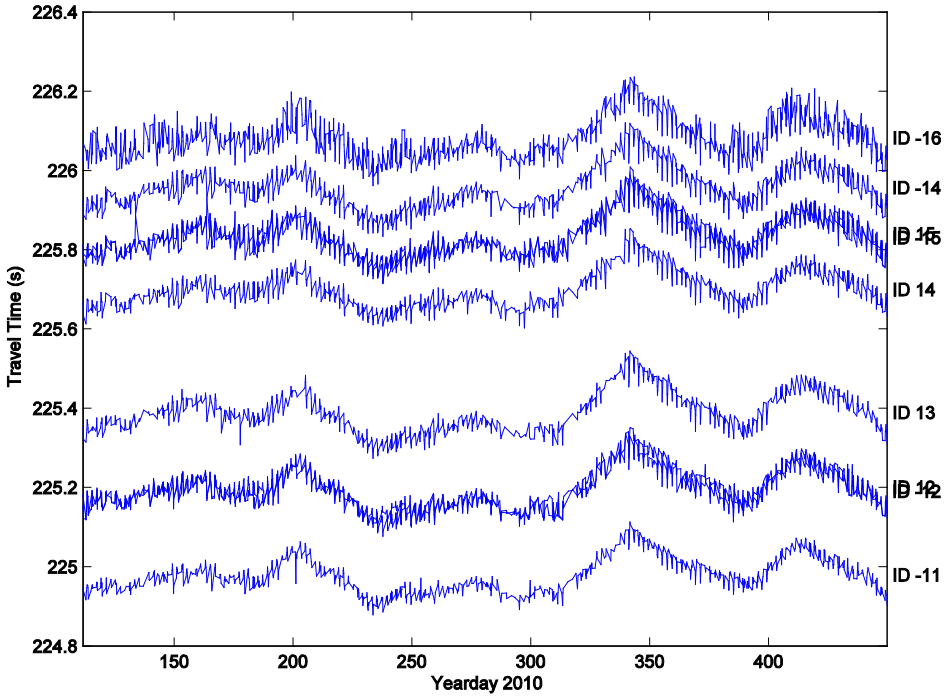

Left vertical axis informed travel time in second, right vertical axis informed the ID number of the rays, and the horizontal axis is year days of 2010

Once we eliminated the effect of tide and eddies from acoustic travel time from T4 to T5, we could isolate the stochastic internal wave effects on our

acoustic signal travel time. We found that there was a small perturbation in travel time throughout the research period (Figure 13).

Figure 13. Effect of Stochastic Internal Wave on Acoustic Travel Time

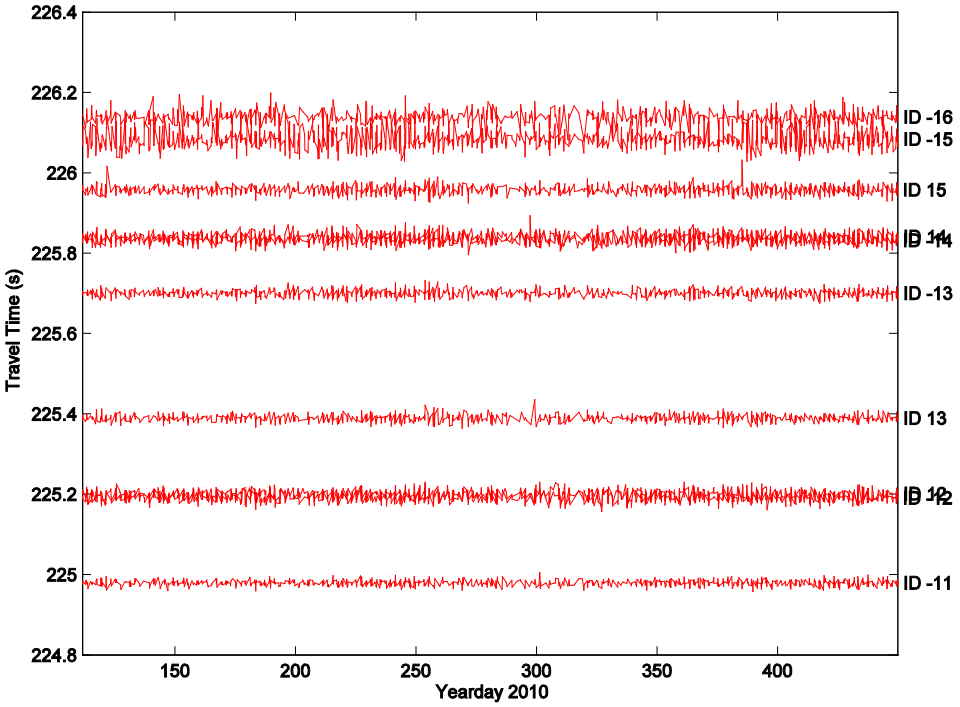

X-axis shows year days of 2010, left y-axis shows the travel time in seconds, and right y-axis shows the ID number of the eigenrays.

By computing the remaining travel time variance of research data, we determined that, in the research area, the effects of tides contribute more at depths shallower than 500 m. Tide effects become less dominant compared to stochastic internal waves at depths deeper than 500 m (Figure 14). The travel time variance plotted as a function of the upper turning point's depth makes it easier to understand the spatial dimension of the rays. Because each ray ID has its own mean upper turning point, this method keeps the rays distinct.

This chapter so far has focused on transmissions between T4 and T5. However, the study was interested in all possible pairs available through the research, including transmissions between T1, T2, T3, and T6.

Figure 14. Travel Time Variance

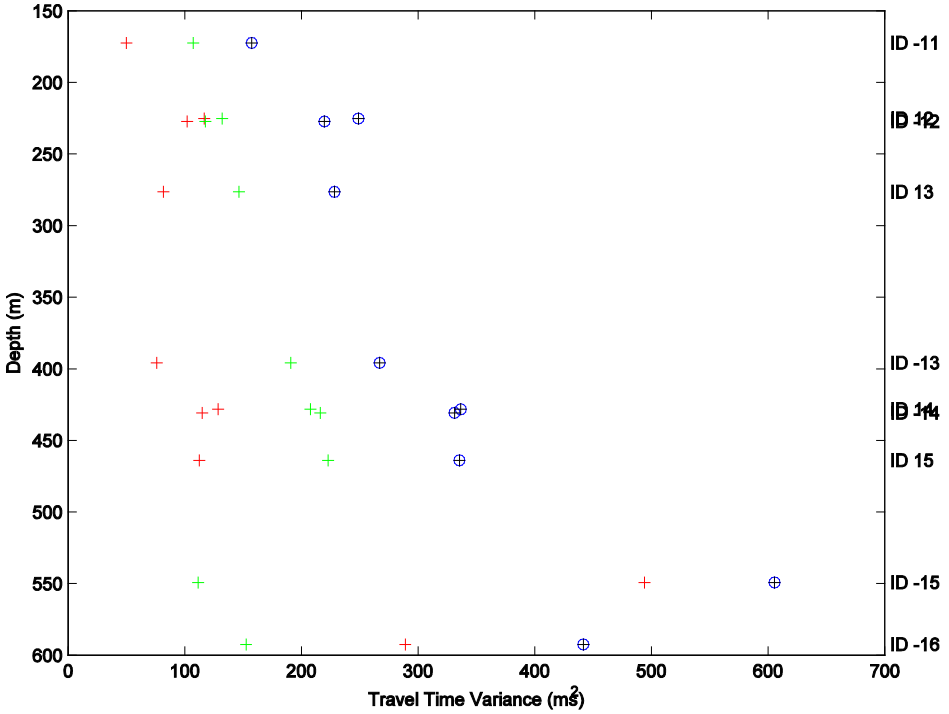

Mean travel time variance of acoustic propagation from T4 to T5. The red (+) shows stochastic internal wave variance, the green (+) shows internal tide variance and blue circle with (+) shows total variance. Left y-axis shows depth in m, right y-axis shows ID number, and x-axis shows travel time variance in ms^{-2}

A. OVERALL TRAVEL TIME VARIANCE

The travel times of the rays that have turning points near the surface have lower variance compared to the rays that have deeper turning points. This might be because the internal wave was located near the acoustic propagation axis, and gave more vertical distribution of sound speed near the propagation axis. As a result, we have more variability near the propagation axis than near the surface (Figure 15). The average rms travel time is 7.03 ms, which provides an rms phase of about 11.04 rad/sec.

The variability of rays moving between N/NE and S/SW was higher compared to other directionalities (Table 5). This can be understood by looking at the geographic position, where we have the Luzon Strait West of the research area. This channel generated internal waves, which propagated to the east, into

the research area. Since the acoustic waves moving between N/NE and S/SW propagate perpendicular to the strait-generated internal wave front, the travel time variabilities of acoustic propagation with roughly N-S directionality are higher compared to other directionalities.

Figure 15. Travel Time Variability Due to Random Internal Wave

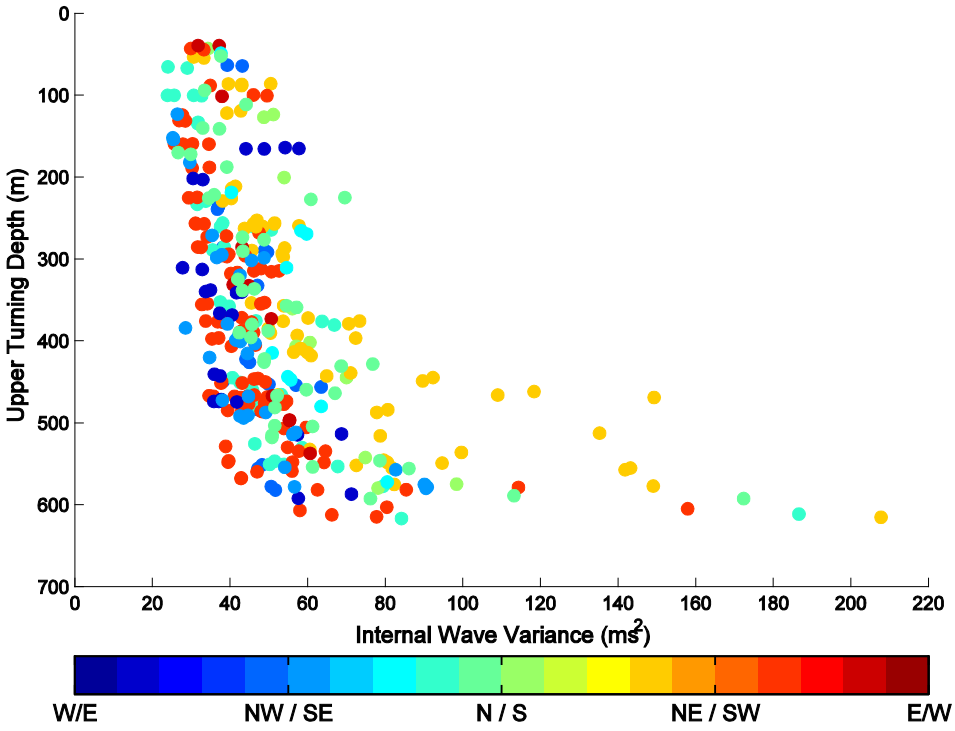

Y-axis shows depth in meter, x-axis shows travel time variance in ms^{-2}, and color map show the direction of the acoustic propagation. The variance is scaled linearly to the 200km-range.

Table 5. RMS Travel Time and Phase RMS

Direction in Deg	-80.53	-52.11	-42.63	-23.68	-14.21	-4.74	4.74	33.16	61.58	80.53
Rms TT (ms)	6.33	6.77	6.23	7.46	7.01	7.71	7.88	8.09	6.42	6.51
Rms Phase (rad/sec)	9.94	10.63	9.79	11.71	11.01	12.11	12.38	12.70	10.08	10.22

The directions are computed relatively from the north. There are 20 classes from west to the east, and only 10 classes have data. The highest travel time variability occurs in the 33.16° direction of propagation, with an rms travel time of 8.09 ms.

Compared to the random internal wave, the internal tide is dominant near the surface and less dominant below 500m depth. The average rms travel time is 5.24 ms. Looking at the tide variance (Figure 16), it is obvious that the rays moving between N/NE and S/SW have much higher variance compared to other directionalities. It is confirmed that the source of internal tides in the Philippine Sea is the Luzon Strait west of the research area.

Figure 16. Travel Time Variability Due to Internal Tide

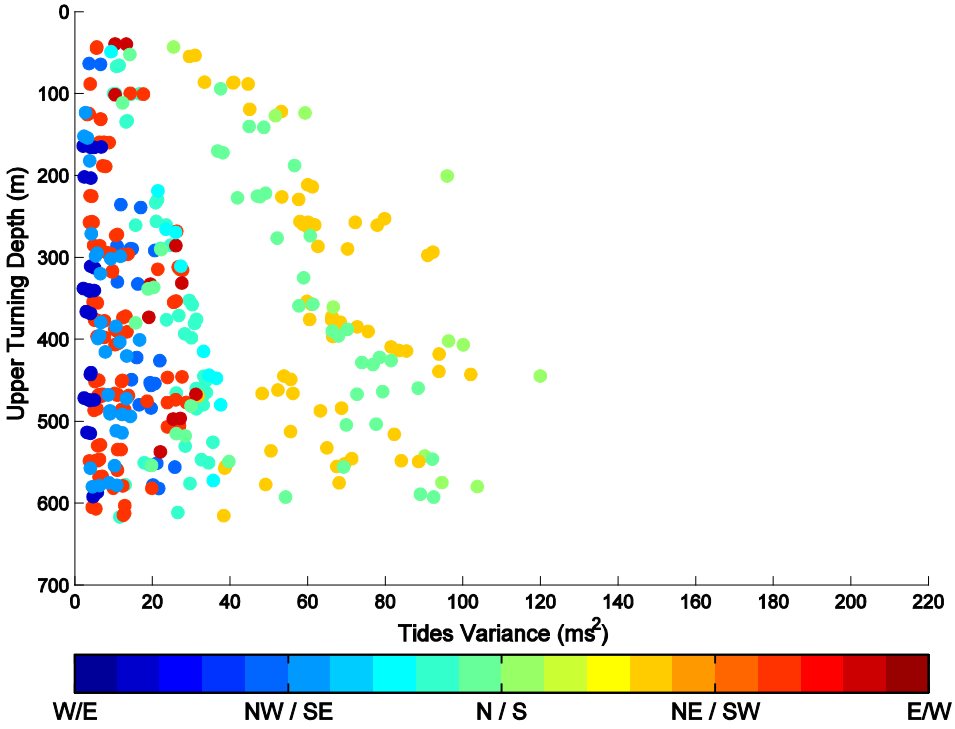

Y-axis shows depth in meters, x-axis shows travel time variance in ms^{-2}, and color mapping shows the direction of the acoustic propagation. The variance is scaled quadratic to the 200km-range.

The eddies contribution to even higher variability of acoustic wave travel time during the research period. There was no dominant directionality of travel time variance due to the circulation of eddies (Figure 17). The average rms travel times for the eddies were 21.60 ms.

Figure 17. Travel Time Variability Due to Eddies

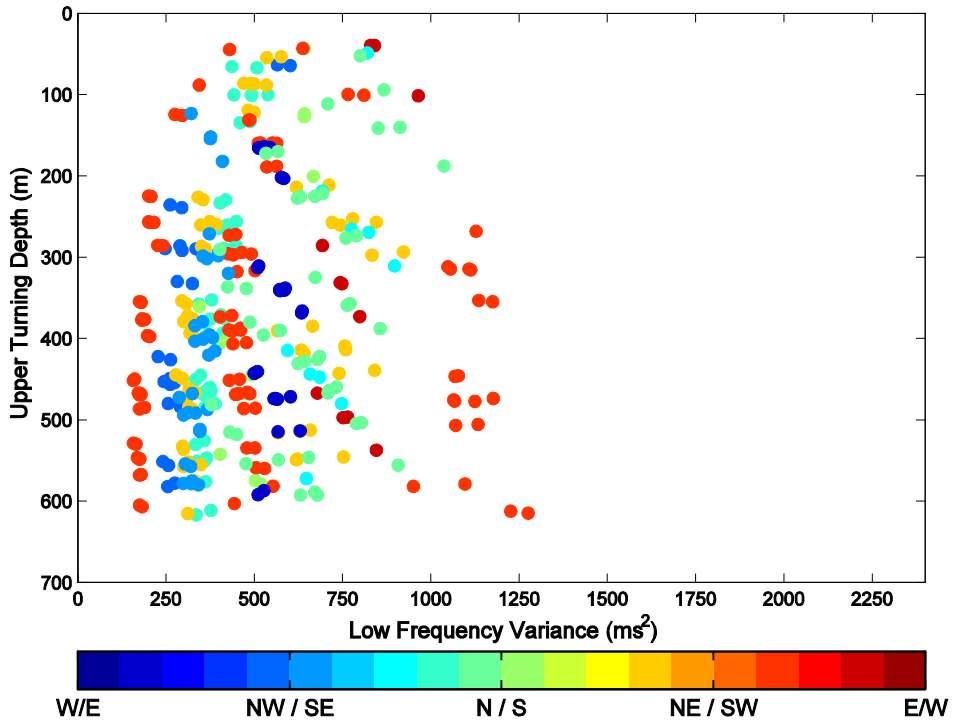

Y-axis shows depth in meters, x-axis shows travel time variance in ms^{-2}, and color mapping shows the direction of the acoustic propagation. The variance is scaled quadratic to the 200km-range

B. SEASONAL TRAVEL TIME VARIANCE

During summer the travel time variability becomes lower. The rms travel time during this period is about 6.82 ms. This weakening process can be understood because the ocean surface receives heat from the sun and pushes the surface mixed layer deeper than during other seasons. As the season changes to fall the variabilities become stronger and stronger. During fall, the rms travel time becomes 6.97 ms; during winter the rms travel time is about 7.37 ms; during spring it is about 7.08 ms (Figure 18).

Even though rms travel time during spring is high compared to fall and summer rms travel times, the travel time variability near the surface during spring is the lowest compared to all. This low value near the surface in spring is

compensated for by variability near the acoustic propagation axis, which is as high as travel time variability during winter (Figure 19).

Figure 18. Seasonal Travel Time Variance Due to Random Internal Wave

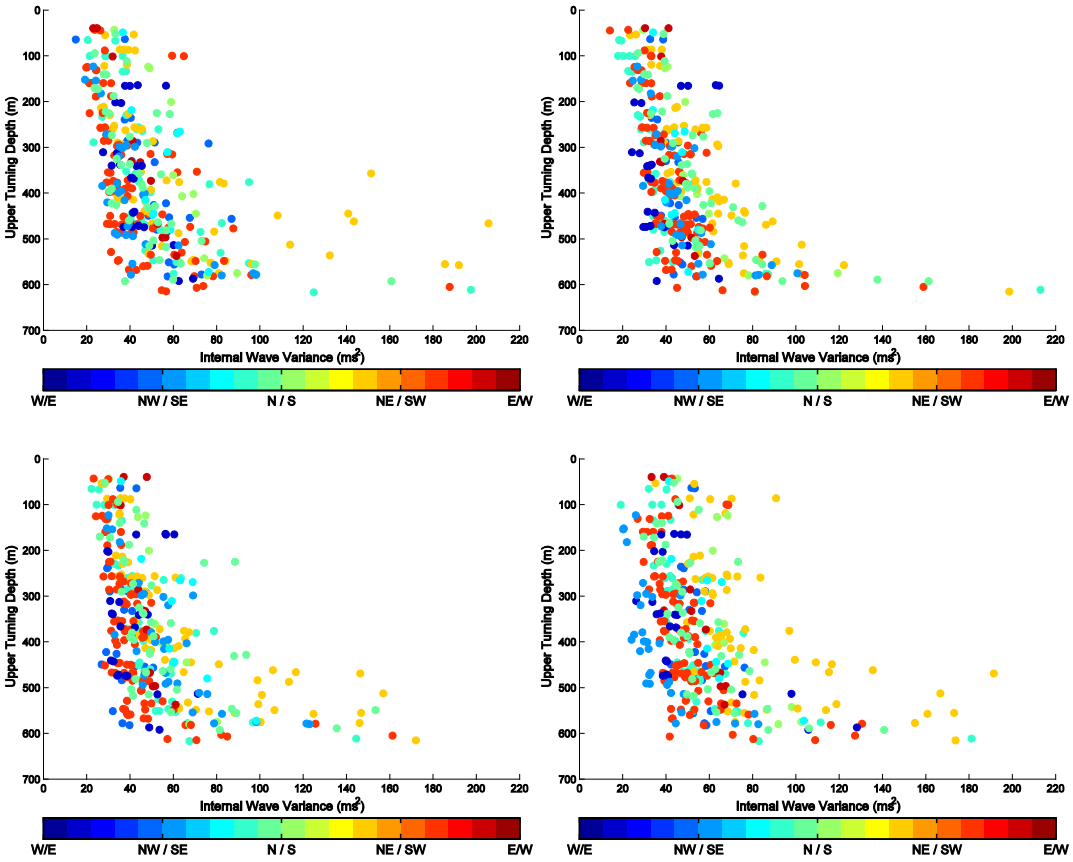

Upper left panel shows internal wave variabilities during Spring 2010, upper right panel shows Summer 2010, lower left panel shows Fall 2010, and lower right panel shows Winter 2011. For every panel Y-axis shows depth in meter, x-axis shows travel time variance in ms^{-2}, and color mapping shows the direction of the acoustic propagation.

Overall the strongest travel time variances are associated with directionality of N/NE and S/SW. These patterns also occur during seasonal observation. However, during summer the strongest travel time variance tends to be associated more strictly with N/S propagation as shown at Table 6.

Figure 19. Seasonal Travel Time Variance Due to Random Internal Waves

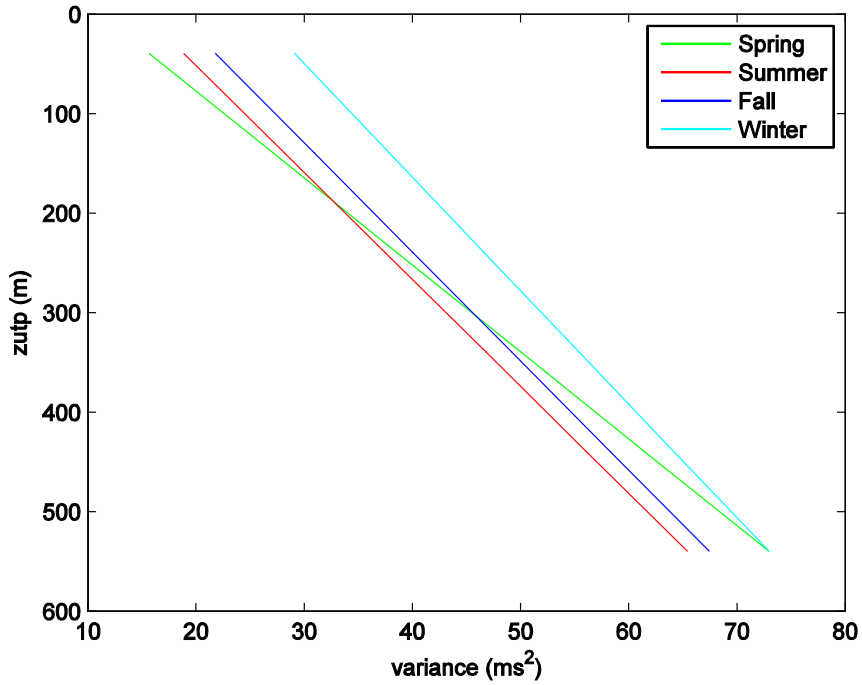

Y-axis shows depth of upper turning point in meters and x-axis shows travel time variance in ms^{-2}.

Table 6. Seasonal RMS Travel Time

Dir	-80.53	-52.11	-42.63	-23.68	-14.21	-4.74	4.74	33.16	61.58	80.53
Spring	6.32	7.26	5.93	7.37	7.40	7.21	7.93	8.55	6.32	6.33
Summer	5.94	6.55	6.30	6.63	6.44	7.89	7.58	7.54	6.43	6.20
Fall	6.23	6.10	6.98	7.90	7.06	7.66	7.44	7.92	6.22	6.57
Winter	6.81	7.40	5.57	7.90	7.39	7.87	8.60	8.78	6.73	6.97

The directions are computed relatively from the north. There are 20 classes from west to the east, and only 10 classes have data. The highest travel time variability occurs in class of 33.16° (between N/S to NE/SW) direction of propagation, but during summer the highest travel time variability at class of -4.74 (near N/S direction).

C. TYPHOON PERIOD TRAVEL TIME VARIANCE

The study uses two typhoons to describe how the acoustic signal travel time variability responds to typhoon. The first were chosen is Typhoon Basyang and the second is Typhoon Juan. These typhoons were chosen because Basyang was a Category 1 Typhoon and Juan was a Category 5 Typhoon.

1. Typhoon Basyang / Conson, July 2010, Category 1

The Typhoon Basyang formed 11 July 2010 and dissipated 18 July 2010. It travelled south from the research area moving from east to west and hit Luzon Island. The typhoon's speed reached 150 km/h and it was categorized as a Typhoon Category 1.

Figure 20. Travel Time Variability during Typhoon Basyang

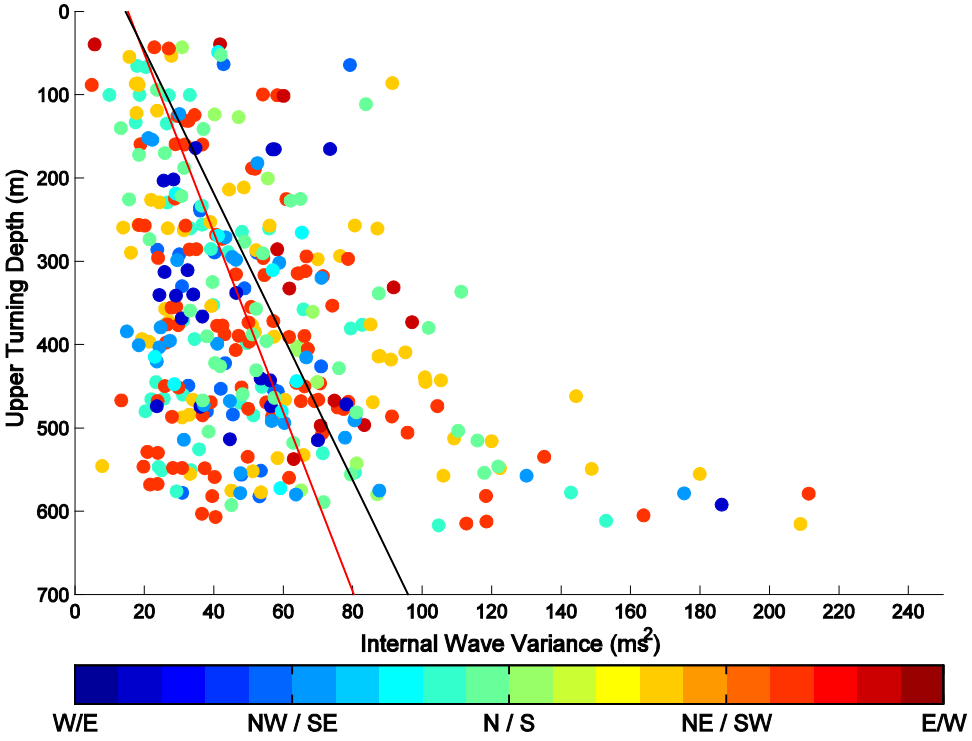

Red line represents the variance trend during Summer 2010 and the black line represents the variance trend during the typhoon period. X-axis shows random internal waves variability in ms^2. Y-axis shows depth in meters and color mapping shows the direction of the acoustic propagation.

The typhoon did not contribute much to the travel time variabilities near the surface. The mean variabilities of travel time during the typhoon period remained similar to the mean travel time variabilities of the summer season. Nevertheless there was some increasing variance near the acoustic propagation axis (Figure 20).

The variance of travel time was distributed evenly across all directionalities. There was not any particular directionality dominant in travel time variance. Horizontally, the typhoon's effect on travel time variables (e.g., salinity, temperature) was also evenly distributed. However, we still could still find traces of internal waves near a depth of 600 m.

2. Typhoon Juan / Megi, Oct 2010, Category 5

Typhoon Juan formed 12 October 2010 and dissipated 24 October 2015. It traveled south of the research area, moving from east to west and hit Luzon Island. The highest speed of the typhoon was 295 km/h and it was categorized as a Typhoon Category 5.

Similar to Typhoon Basyang, Typhoon Juan did not add any significant change to the existing travel time variabilities. The average variability during the typhoon period remained similar to average variability during fall 2010. But as Typhoon Basyang had done, Typhoon Juan destroyed the horizontal structure of sound speed, so it was hard to determine dominant variability based on directionality during Typhoon Juan (Figure 21)

The variability near the acoustic propagation axis slightly reduced during the typhoon. This can be understood as the result of typhoon's strength and ability to penetrate into deeper water. As a result sound speed distribution at that depth was disrupted and there was lower variability of the acoustic travel time during Typhoon Juan.

Figure 21. Travel Time Variabilities during Typhoon Basyang

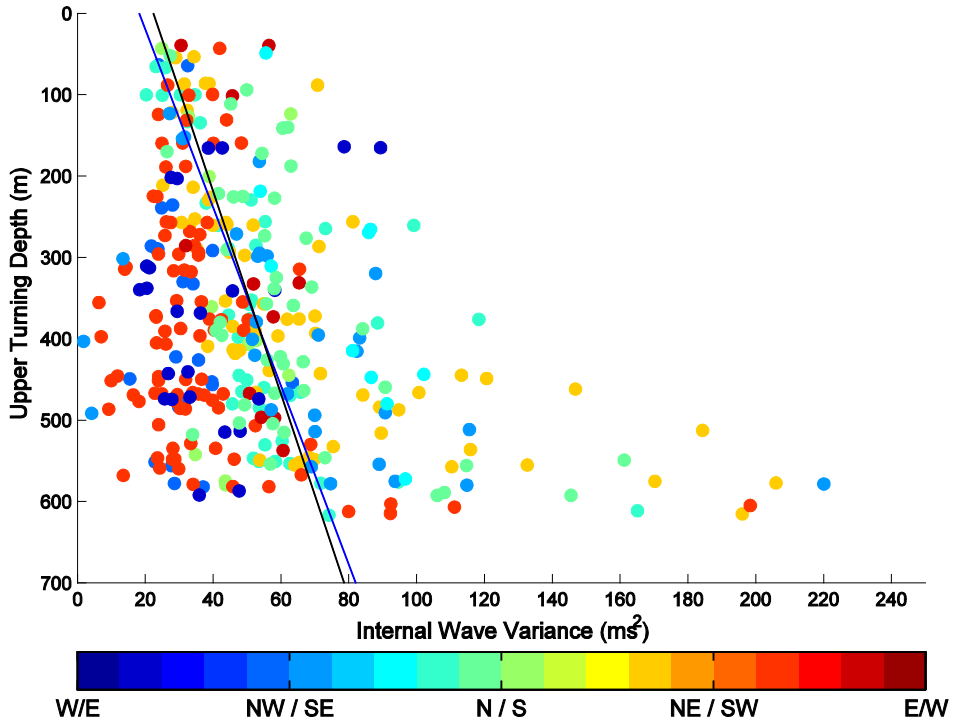

Blue line represents the variance trend during Fall 2010 and the black line represents the variance trend during the typhoon period. X-axis shows random internal waves variability in ms^2. Y-axis shows depth in meters and color mapping shows the direction of the acoustic propagation.

The travel time variability observed in this chapter will be compared to theoretical models in the following chapter. Can the theoretical results be used to predict real situations in the Philippine Sea?

THIS PAGE INTENTIONALLY LEFT BLANK

V. PREDICTED TRAVEL TIME STATISTICS

The question to be addressed in this chapter is: How accurately can we predict travel time variances using the theory from Chapter II and the Garret Munk internal waves spectrum? Using standard parameters from the Garret Munk model, predictions from the theory are compared to the observations in Figure 22. Both the theory and the observations have been scaled to 200-km range.

Figure 22. Data and Travel Time Variance Using GM Internal Wave Spectrum

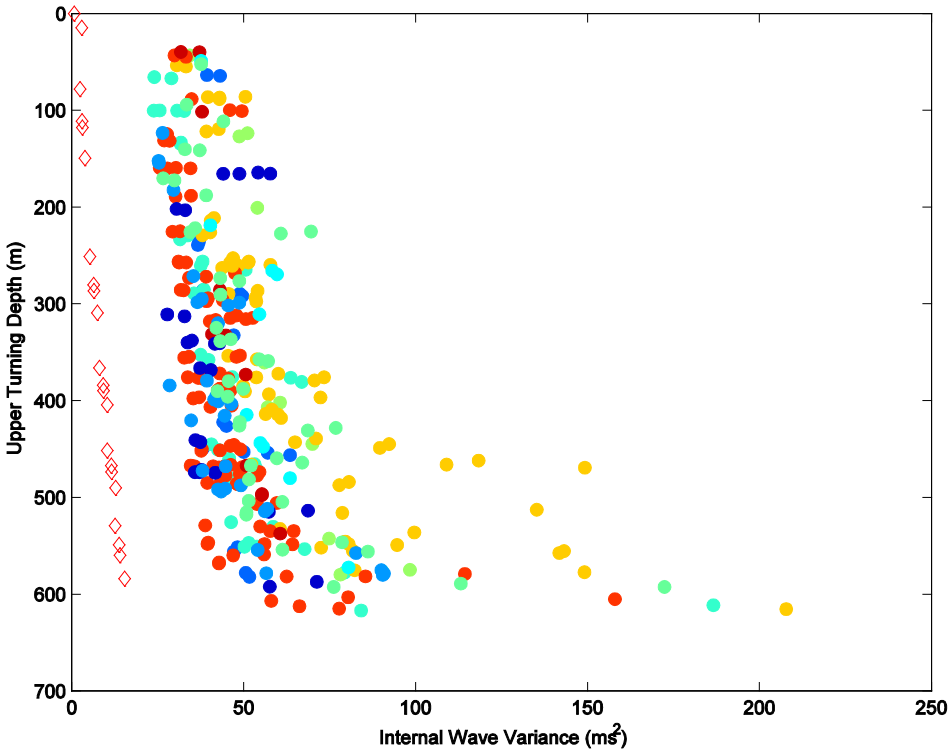

Scattered dots show the research data travel time variance. The red diamonds predict travel time variance using the Garret Munk internal wave spectrum model. Theory and observation have been scaled to a 200-km range.

The theory's predictions of travel time variance are low by a factor of 5 or more. Changing the internal wave energy by a factor of 2 (ζ_0=10.32), and reducing the modal bandwidth factor j_* to 1 yields a better comparison, as seen in Figure 23.

Figure 23. Data and Travel Time Variance Using Adjusted GM Internal Wave Spectrum

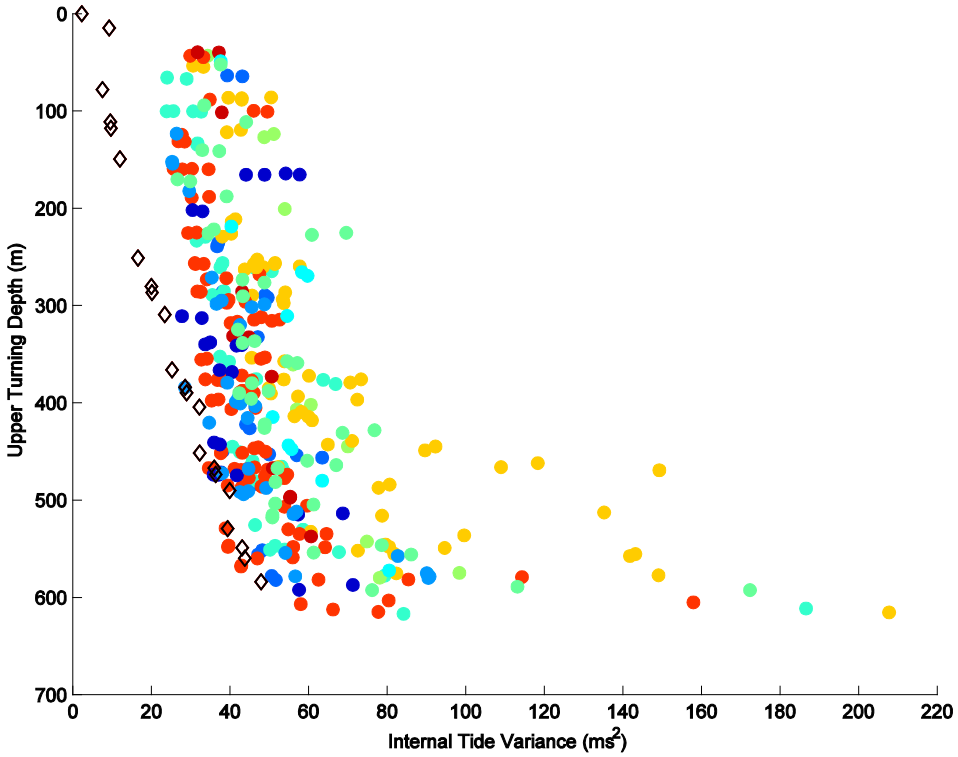

Scattered dots show the research data travel time variance. The black diamond predicted travel time variance using GM internal wave spectrum model. Theory and observation have been scaled to a 200-km range.

The theory is seen to do a better job predicting deep turning point rays. The rays turning near the sea surface are significantly off. Possible explanations are as follows. We know that the GM model was formulated based on observations in the main thermocline and therefore it is not accurate for describing internal waves near the sea surface. Also the theory described in Chapter II has approximations. One big approximation is the ray tangent

approximation in which the ray is assumed to be locally straight over an internal-wave correlation length. This approximation is less accurate for higher angle rays that have shallower turning depths, and it is a bad approximation near the ray turning depth where the ray has maximum curvature.

THIS PAGE INTENTIONALLY LEFT BLANK

VI. CONCLUSION AND FUTURE DIRECTION

The overall rms travel times variance caused by eddies, internal tides, and internal waves in the Philippine Sea during the research period are roughly 21 ms, 5 ms, and 7 ms respectively. The research revealed that internal tides were more important for acoustic travel time variance at depths shallower than 500 m, and random internal waves were more important at depths deeper than 500 m. Overall, eddies cause the highest travel time variance. The highest travel time variability from internal waves occurs during winter, followed by spring, fall and summer. During spring, variability near the surface was lowest compared to all other seasons. Horizontal anisotropy was observed during the research period. The highest travel time variance can be seen in acoustic propagation with a directionality moving between N/NE and S/SW. However, during summer the strongest travel time variance tends to be associated more strictly with N/S propagation. For typhoons, during the research period, there was not much change in the magnitude of travel time variance, but typhoons destroyed the horizontal structure of anisotropy.

Based on the theory from Chapter II and the Garret Munk Internal Wave Spectrum Model, the variability in the Philippine Sea during the research period can be estimated. As a function of distance, the theory predicts that the internal wave travel time variance will grow as the distance between transmitter and receiver increases, and this is consistent with the observations of this research. The theory also predicts that internal wave travel time variance will be horizontally isotropic and this point is also consistent with these research observations. However, using standard Garret Munk parameters, the theory under-predicts the observed travel time variance by a factor of 5 or more due to it was formulated based on observations in the main thermocline and the ray is assumed to be locally straight over an internal-wave correlation length.

In the future we can work on how to estimate travel time variances from internal tides, and we can work on improving the internal wave theory.

THIS PAGE INTENTIONALLY LEFT BLANK

LIST OF REFERENCES

Bell, T. H., 1975: Topographically generated internal waves in the open ocean. *J. Geophysical Research,* **80**, 320–327, doi:10.1029/JC080i003p00320.

Colosi, J. A., 2015: Sound Propagation through the Stochastic Ocean (manuscript submitted for publication with Cambridge University Press).

Colosi, J. A., T. K. Chandrayadula, A. G. Voronovich, and V. E. Ostashev, 2013: Coupled mode transport theory for sound transmission through an ocean with random sound speed perturbations: Coherence in deep water environments. *J.Acoust.Soc.Am.,* **134**, 3119–3133, doi:http://dx.doi.org/10.1121/1.4818779.

Colosi, J. A., L. J. Van Uffelen, B. D. Cornuelle, M. A. Dzieciuch, P. F. Worcester, B. D. Dushaw, and S. R. Ramp, 2013: Observations of sound-speed fluctuations in the western Philippine Sea in the spring of 2009. *J.Acoust.Soc.Am.,* **134**, 3185–3200, doi:http://dx.doi.org/10.1121/1.4818784.

Dushaw, B. D., 2008: Another look at the 1960 Perth to Bermuda long-range acoustic propagation experiment. *Geophys.Res.Lett.,* **35**, doi:10.1029/2008GL033415.

Farmer, D., Q. Li, and J. Park, 2009: Internal wave observations in the South China Sea: The role of rotation and non-linearity. *Atmosphere-Ocean,* **47**, 267–280, doi:10.3137/OC313.2009.

Flatté, S. M., 1979: *Sound transmission through a fluctuating ocean.* Cambridge monographs on mechanics and applied mathematics, Cambridge University Press, 299 pp.

Garrett, C., E. Kunze, 2007: Internal tide generation in the deep ocean. *Annu.Rev.Fluid Mech.,* **39**, 57–87, doi:10.1146/annurev.fluid.39.050905.110227.

Garrett, C. W. Munk, 1975: Space-time scales of internal waves: A progress report. *J. Geophysical Research,* **80**, 291–297, doi:10.1029/JC080i003p00291.

Google, 2015: *Philippine Sea*, 20°16’11.21” N and 125°30’49.79” E, Google Earth, accessed 21 June 2015.

Google, 2015: *Philippine Sea*, 20°11’17.69” N and 127°19’18.16” E, Google Earth, accessed 21 June 2015.

Muller, P., 1976: On the diffusion of momentum and mass by internal gravity waves. *J.Fluid Mech.,* **77**, 789–823, doi:10.1017/S0022112076002899.

Munk, W.H., and Zachariasen, F. 1976. Sound propagation through a fluctuating stratified ocean: Theory and observation. *J. Acoust. Soc. Am*., 59, 818–838.

Nakano, T., I. Kaneko, M. Endoh, and M. Kamachi, 2005: Interannual and decadal variabilities of npiw salinity minimum core observed along JMA's Hydrographic Repeat Sections. *J.Oceanogr.,* **61**, 681–697, doi:10.1007/s10872-005-0076-5.

NOAA, 2015: Harmonic constituents for 9410170, San Diego CA. [Available online at http://tidesandcurrents.noaa.gov/harcon.html?id=9410170&type=].

Pierce, A. D., 1989: *Acoustics: An introduction to its physical principles and applications.* 1989th ed. Acoustical Society of America, 678 pp.

Qiu, B., S. Chen, 2010; 2010: Interannual variability of the North Pacific Subtropical Countercurrent and its associated mesoscale eddy field. *J.Phys.Oceanogr.,* **40**, 213–225.

Ramp, S. R., J. A. Colosi, P. F. Worcester, F. L. Bahr, K. D. Heaney, J. A. Mercer, and L. J. Van Uffelen, 2014: Direct observations of the mesoscale variability in the western Philippine Sea (manuscript submitted for publication with *J.Phys.Oceanogr).*

Rudnick, D. L., S. Jan, L. Centurioni, C. M. Lee, R. C. Lien, J. Wang, D. K. Lee, R. S. Tseng, Y. Y. Kim, and C. S. Chern, 2011: Seasonal and mesoscale variability of the Kuroshio near its origin. *Oceanography,* **24**, 52–63, doi:http://dx.doi.org/10.5670/oceanog.2011.94.

Watson, K. M., B. J. West, and B. I. Cohen, 1976: Coupling of surface and internal gravity waves: a mode coupling model. *J.Fluid Mech.,* **77**, 185–208, doi:10.1017/S0022112076001195.

Worcester, P. F., M. A. Dzieciuch, J. A. Mercer, R. K. Andrew, B. D. Dushaw, A. B. Baggeroer, K. D. Heaney, D&apos, G. L. Spain, J. A. Colosi, R. A. Stephen, J. N. Kemp, B. M. Howe, L. J. Van Uffelen, and K. E. Wage, 2013: The North Pacific Acoustic Laboratory deep-water acoustic propagation experiments in the Philippine Sea. *J.Acoust.Soc.Am.,* **134**, 3359–3375, doi:http://dx.doi.org/10.1121/1.4818887.

Zhao, Z., 2014: Internal tide radiation from the Luzon Strait. *Journal of Geophysical Research: Oceans,* **119**, 5434–5448, doi:10.1002/2014JC010014.

INITIAL DISTRIBUTION LIST

1. Defense Technical Information Center
   Ft. Belvoir, Virginia

2. Dudley Knox Library
   Naval Postgraduate School
   Monterey, California